REPORT DOCUMENTATION PAGE

AFRL-SR-AR-TR-04-

0182

1. REPORT DATE *(DD-MM-YYYY)*	2. REPORT TYPE	3. DATES COVERED *(From - To)*
04/22/2004	Final	04/01/1999 - 09/30/2002

4. TITLE AND SUBTITLE
Feasibility of Spectral Holeburning Memories and Processors

For Space-Based Applications

5a. CONTRACT NUMBER

5b. GRANT NUMBER
F49620-99-1-0224

5c. PROGRAM ELEMENT NUMBER

6. AUTHOR(S)
Dr. Selim Shahriar, Prof. Shaoul Ezekiel, Prof. Cardinal Warde

5d. PROJECT NUMBER
2305/DX

5e. TASK NUMBER

5f. WORK UNIT NUMBER

7. PERFORMING ORGANIZATION NAME(S) AND ADDRESS(ES)

Research Laboratory of Electronics
Massachusetts Institute Of Technology
77 Massachusetts Avenue
Cambridge, MA 02139

8. PERFORMING ORGANIZATION REPORT NUMBER

9. SPONSORING / MONITORING AGENCY NAME(S) AND ADDRESS(ES)
Air Force Office of Scientific Research
4015 Wilson Boulevard
Arlington, VA 22203-1954

20040423 045

NUMBER(S)

12. DISTRIBUTION / AVAILABILITY STATEMENT
Distribution Statement A: unlimited

13. SUPPLEMENTARY NOTES

14. ABSTRACT

The purpose of this research was to explore the feasibility of using spectral hole-burning (SHB) memories for caching and processing large amounts of high-speed imagery data that are expected in future space-based surveillance systems. The research was to consist of three parts. First, the power of spectral holeburning for image-based storage and processing was to be illustrated by performing several demonstration experiments, using Raman excited spin coherence (RESC). Second, the properties of Raman excited spin coherences were to be used to increase the operating temperature of spectral holeburning materials. Third, long term storage of very high volume of optical data was to be demonstrated via frequency domain spectral holeburning in an organic dye embedded in a host of PMMA. In pursuing application of RESC, we have demonstrated that nitrogen-vacancy color centers in diamond is a viable medium for SHB memory. Furthermore, we have demonstrated, for the first time in a solid, the slowing and halting of light pulses in a crystal of Pr:YSO. This effect has spawned a wide range of activities in the research community, and has a range of application including optical data buffering and high-fidelity quantum memory. For high volume storage systems, it became clear early on that the objectives of this project could be better met by simple variations of the tasks originally envisioned. Specifically, we realized that an organic dye called Phenanthraquinone doped in PMMA could achieve the same storage capacity as envisioned for the SHB medium, with a key advantage that it could be used at room

15. SUBJECT TERMS

16. SECURITY CLASSIFICATION OF:			17. LIMITATION OF ABSTRACT	18. NUMBER OF PAGES	19a. NAME OF RESPONSIBLE PERSON
a. REPORT	b. ABSTRACT	c. THIS PAGE			19b. TELEPHONE NUMBER *(include area code)*

Feasibility of Spectral Holeburning Memories and Processors for Space-Based Applications

Grant# : F49620-99-1-0224
OSP#: 6829700

FINAL REPORT

Co-Principal Investigators:
Dr. Selim Shahriar, Prof. Shaoul Ezekiel, and Prof. Cardinal Warde,
Research Laboratory of Electronics, MIT

ABSTRACT

The purpose of this research was to explore the feasibility of using spectral hole-burning (SHB) memories for caching and processing large amounts of high-speed imagery data that are expected in future space-based surveillance systems. The research was to consist of three parts. First, the power of spectral holeburning for image-based storage and processing was to be illustrated by performing several demonstration experiments, using Raman excited spin coherence (RESC). Second, the properties of Raman excited spin coherences were to be used to increase the operating temperature of spectral holeburning materials. Third, long term storage of very high volume of optical data was to be demonstrated via frequency domain spectral holeburning in an organic dye embedded in a host of PMMA. In pursuing application of RESC, we have demonstrated that nitrogen-vacancy color centers in diamond is a viable medium for SHB memory. Furthermore, we have demonstrated, for the first time in a solid, the slowing and halting of light pulses in a crystal of Pr:YSO. This effect has spawned a wide range of activities in the research community, and has a range of application including optical data buffering and high-fidelity quantum memory. For high volume storage systems, it became clear early on that the objectives of this project could be better met by simple variations of the tasks originally envisioned. Specifically, we realized that an organic dye called Phenanthraquinone doped in PMMA could achieve the same storage capacity as envisioned for the SHB medium, with a key advantage that it could be used at room temperature. As such, we pursued the development of this technology ardently under this program, and developed a novel device called the super-parallel holographic optical correlator that is likely to be of near term practical usage in space-borne applications such as missile recognition and tracking. We have also shown how this device can be operated as a high-speed holographic RAM when operated in reverse. We have also shown how holograms based on this material can be used to realize a high speed holographic stokesmeter, which in turn can be employed for polarization imaging capable of discriminating between plumes and rocket bodies during the boost phase of a rocket launch. The device can also perform shape discrimination without imaging.

REPORT DOCUMENTATION

1. LIST OF PUBLICATIONS AND MANUSCRIPTS:

Published in Journals:

1. "Demonstration of a Super-Parallel Holographic Optical Correlator for Ultrafast Database Search," M.S. Shahriar, M. Kleischmit, R. Tripathi, and J. shen, *Opt. Letts.* **28,** 7, pp. 525-527(2003)
2. "Coherent and incoherent beam combination using thick holographic substrates," M.S. Shahriar; J. Riccobono; M. Kleinschmit; J.T. Shen, Opt. Commun., **220**, 1, pp. 75-83(2003).
3. "Raman Excited Spin Coherence in NV-Diamond," P.R. Hemmer, A.V. Turukhin, M.S. Shahriar, and J.A. Musser, *Opt. Letts.* **26**, 6 (2001).
4. "Simultaneous Operation of A Super-Parallel HolographicOptical Correlator and a Super-Parallel Holographic RAM," M.S. Shahriar, J. Shen, R. Tripathi, and M. Huq, to appear as an invited paper for the Special Issue of Optical Engineering on Trends in Pattern Recognition Algorithms, Architectures, and Devices, 2004.
5. "Observation of Ultraslow and Stored Light Pulses in a Solid," A. V. Turukhin, V.S. Sudarshanam, M.S. Shahriar, J.A. Musser, B.S. Ham, and P.R. Hemmer, *Phys. Rev. Lett.* **88**, 023602 (2002).
6. "Observation of sub-kilohertz resonance in Rf-optical double resonance experiment in rare earth ions in solids," M.K. Kim, B.S. Ham, P.R. Hemmer, and M.S. Shahriar, J. Mod. Optic **47**, 10 (2000).
7. "Ultra-fast Holographic Stokesmeter for Polarization Imaging in Real Time," M.S. Shahriar, J. shen, R. Tripathi, M. Kleischmit, and T. Nee, to appear in *Opt. Letts.*

Conference Presentations:

1. M.S. Shahriar, J. Riccobono, W. Weathers, "Holographic Beam Combiner," International Microwaves and Optics Conference, Rio De Janeiro, Brazil, 1999.
2. B. Ham, M.S. Shahriar, and P.R. Hemmer, ""Efficient Phase Conjugation using Raman dark resonances in an optically dense solid," Conference on L asers and Electro-Optics, Baltimore, MD, 1999.
3. B. Ham, M.S. Shahriar, and P.R. Hemmer, ""Electromagnetically induced transparency over spectral hole-burning temperature in an inhomogeneously broadened solid," Conference on L asers and Electro-Optics, Baltimore, MD, 1999.
4. B. Ham, M.S. Shahriar, and P.R. Hemmer, "Observation of Laser Jitter Enhanced Hyperfine Spectroscopy," OSA Annual Meeting, Santa Clara, CA, 1999.
5. B. Ham, M.S. Shahriar, and P.R. Hemmer, "Enhancement of Four-wave-mixing and Line-narrowing using EIT in an optically dense double-lambda solid," OSA Annual Meeting, Santa Clara, CA, 1999.
6. M.K. Kim, B. Ham, M.S. Shahriar, and P.R. Hemmer, "Sub-kHz resonance structure in rf-optical double resonance of rare-earth ions in solids," OSA Annual Meeting, Santa Clara, CA, 1999.

7. P.R. Hemmer, M.S. Shahriar, and A. Turukhin, "Raman excited spin coherences for high-temperature spectral hole-burning memories" Conference on L asers and Electro-Optics, San Francisco, CA, 2000

8. P.R. Hemmer, A. Turukhin, M.S. Shahriar, and J.A. Musser, "Raman Excited Spin Coherence in NV Diamond," Optical Society of America Annual Meeting, Providence, RI, October 2000 **(postdeadline)**

9. P.R. Hemmer, A. Turukhin, M.S. Shahriar, and J.A. Musser, "Raman Excited Spin Coherence in NV Diamond," presented at the International Quantum Electronics Conference, Baltimore, MD, May 2001.

10. "Observation of Ultraslow Group Velocity of Light in a Pr:YSO crystal," V.S. Sudarshanam, M.S. Shahriar, and P.R. Hemmer, *31st Winter Colloquium in Quantum Electronics*, Snowbird, Utah (Jan 2001).

11. "First Observation of Ultraslow Group Velocity of Light in a Solid," A. Turukhin, V.S. Sudarshanam, M.S. Shahriar, J.A. Musser, and P.R. Hemmer, proceedings of the *International Quantum Electronics Conference*, Baltimore, MD, 2001.

12. "Spin Mediated Slowing and Stoppage of Light in a Solid," A.V. Turukhin, M.S. Shahriar, J.A. Musser, and P.R. Hemmer, *proceedings of Spintech 1*, Maui, Hawaii, 2001.

13. "First Observation of Ultraslow Group Velocity of Light in a Solid," A. Turukhin, V.S. Sudarshanam, M.S. Shahriar, J.A. Musser, and P.R. Hemmer, *proceedings of the SPIE Conference,* San Diego, CA 2001.

14. "Raman Excited Spin Coherence in NV Diamond," P.R. Hemmer, A. Turukhin, M.S. Shahriar, and J.A. Musser, *proceedings of the SPIE Conference,* San Diego, CA 2001 **(Invited)**.

15. "Applications of Slow and Stopped Light in Solid," P.R. Hemmer and M.S. Shahriar, presented at *the Progress in Quantum Electronics conference*, Snowbird, UT, Jan. 2002 **(Invited)**.

16. **"**Demonstration of a Super-Parallel Holographic Optical Correlator for Ultrafast Database Search," M.S. Shahriar, M. Kleinschmit, W. Weathers, and R. Tripathi, (**post-deadline** paper), CLEO 2002.

17. "A Super-Parallel Holographic Correlator for Ultrafast Database Search," M.S. Shahriar, M. Kleinschmit, W. Weathers, J. Donoghue, and J. Shen, presented at the Annual Meeting of the Optical Society of America, Orlando, FL (2002).

18. "Quantum Versus Super-Parallel Holographic Database Search," M.S. Shahriar, presented at the SPIE Aerosense Meeting, Orlando, FL, April 2003.

19. "Ultrafast Database Search Using Holographic Memory Vs. Quantum Computing," M.S. Shahriar, SPIE Photonic West, San Jose, CA, Jan 2003. **(Invited Paper)**.

20. "Imaging Stokesmeter utilizing holographic diffraction gratings," M.S. Shahriar, R. Tripathi, M. Kleinschmit, and T. Nee, presented at CLEO, Baltimore, MD, 2003.

2. REPORT OF INVENTIONS

- *Demonstrated a suepr-parallel holographic optical correlator for ultrafast database search that can be used for missile recognition and tracking*
- *Demosntrated a super-parallel holographic RAM for high speed data recall*
- *Demonstrated s holographic stokes-meter for polarization imaging that can be used for imaging through plumes, as well as for shape discrimination without imaging*
- *Demonstrated slowing and halting of light pulses using Raman excited spin echo in Pr:YSO, with application to data buffering for optical communication, as well as for high fidelity quantum memory*
- *Demonstrated the feasibility of using nitrogen-vacancy color center in diamond as a viable medium for SHB memory*

3. SCIENTIFIC PROGRESS AND ACCOMPLISHMENTS

The purpose of this research was to explore the feasibility of using spectral hole-burning (SHB) memories for caching and processing large amounts of high-speed imagery data that are expected in future space-based surveillance systems. The research was to consist of three parts. First, the power of spectral holeburning for image-based storage and processing was to be illustrated by performing several demonstration experiments, using Raman excited spin coherence (RESC). Second, the properties of Raman excited spin coherences were to be used to increase the operating temperature of spectral holeburning materials. Third, long term storage of very high volume of optical data was to be demonstrated via frequency domain spectral holeburning in an organic dye embedded in a host of PMMA. In pursuing application of RESC, we have demonstrated that nitrogen-vacancy color centers in diamond is a viable medium for SHB memory. Furthermore, we have demonstrated, for the first time in a solid, the slowing and halting of light pulses in a crystal of Pr:YSO. This effect has spawned a wide range of activities in the research community, and has a range of application including optical data buffering and high-fidelity quantum memory. For high volume storage systems, it became clear early on that the objectives of this project could be better met by simple variations of the tasks originally envisioned. Specifically, we realized that an organic dye called Phenanthraquinone doped in PMMA could achieve the same storage capacity as envisioned for the SHB medium, with a key advantage that it could be used at room temperature. As such, we pursued the development of this technology ardently under this program, and developed a novel device called the super-parallel holographic optical correlator that is likely to be of near term practical usage in space-borne applications such as missile recognition and tracking. We have also shown how this device can be operated as a high-speed holographic RAM when operated in reverse. We have also shown how holograms based on this material can be used to realize a high speed holographic stokesmeter, which in turn can be employed for polarization imaging capable of discriminating between plumes and rocket bodies during the boost phase of a rocket launch. The device can also perform shape discrimination without imaging.

3.1 The Super-Parallel Architecture For Holographic Correlation And A Holographic RAM

[see attachment 1 for further details]

It has recently been shown that a quantum computer could be used to factor large numbers efficiently using Shor's algorithm (SA)[1], and to search a database of N elements in $N^{1/2}$ steps using Grover's algorithm (GA)[2]. While SA offers an exponential speedup over the known classical algorithm for factoring, it is yet to be proven that there exists no classical algorithm that is as fast as SA. In contrast, it has been claimed that no classical technique can perform a search as fast as GA. This claim is inaccurate, based on the limiting assumption that a classical search would be carried out in a serial manner. Several groups have shown how GA does not rely on entanglement, but rather is rooted in the parallelism of wave mechanics. Such a parallelism is also present in classical optics. As such, it is eminently plausible that a quadratic speed-up in searching an unsorted database may be implementable using techniques of classical optics. Zubairy et al. recently proposed a quasi-classical technique that can perform a search as fast as GA, using unentangled atoms, and parallelism of optics[3]. Recently, we have demonstrated

experimentally the basic features of a classical search mechanism that is as fast as GA[4-6]. Specifically, this technique is based on super-parallel holography (SPH), which is a variant of the conventional holographic optical correlator (HOC)[7]. While the speed of GA scales the same way as that of these classical and quasi-classical techniques, there is one potentially significant advantage in using GA. Specifically, a quantum computer needed to implement a GA based search of an N-element database requires $O(\log_2 N)$ quantum bits, while any classical or quasi-classical technique requires O(N) bits. However, this seemingly significant advantage of the GA is not of practical interest, because a database searching process is likely to require a storage system with a number of memory bits O(N), even when the searching process itself uses a quantum computer. Thus, for any search technique, including GA, the net resources necessary is O(N). Thus, given a choice of search engines each of which takes $N^{1/2}$ steps, and employs resources O(N), the preference must be based on engineering considerations such as reliability and practicability. In this context, the SPH-based search engine mentioned above may be the preferred one, given that it may be realized for practical applications within a few years, for non-trivial applications such as face recognition or computer vision.

The SPH-based optical correlator (SPHOC), invented under this program[4-6], is a device that performs the holographic optical correlation (HOC) operation simultaneously at thousands of locations, with essentially the same number of detector elements as needed for a single HOC. To see how it performs a search in $N^{1/2}$ steps, consider first the operation of the HOC, which is based on $M= N^{1/2}$ images written in a single location, via angular multiplexing, through interference with a plane wave reference beam. When the query image is applied to this location, a plane wave is produced at the angle corresponding to the matching image, representing a correlation. A detector array containing M elements can be used to determine the identity of the image. Consider next a situation where M different spatial locations are used, each storing M images. Suppose also that the query image is first cloned into M copies[9], and the correlation is carried out simultaneously at each of the M locations. In a simple configuration, one must still use M different detector arrays, each containing M different detector elements. The total number of detector elements one must sort through is $M^2=N$, so that the search still takes O(N) steps. The SPHOC architecture starts with this model, using M-fold cloning of the query image. However, a holographic demultiplexing scheme (HDS) is used at the output of the correlator, in a manner so that only two detector arrays, each containing M detector elements, are necessary: one to identify the location, and the other to identify the angle, of the matched image. Using a holographic memory unit (HMU) which could hold two terabyte (TB) of data[9], in a CD-ROM sized, 1 cm-thick substrate, the SPHOC searching speed may be **as high as one million times faster than a Digital Signal Processing (DSP) based system[6].**

As mentioned, we have already demonstrated the feasibility of the SPHOC on a small scale. However, in order to realize the SPHOC on a non-trivial scale, the HDS requires a large array of microscopic, special-purpose optical components that can be created only using lithographic integrated optics technology. Under this project, we have developed a novel approach for fabricating a custom-designed, inhomogeneous, prism-coupled lenslet array for the HDS stage of the architecture. We have analyzed the actual beam propagation, and calculated the exact design parameters for the prism-lenslet-array. In a future endeavor, the array would be fabricated, and incorporated into a large scale version of the SPHOC.

THE SUPER PARALLEL HOLOGRAPHIC OPTICAL CORRELATOR:

The key feature of the proposed work is the SPHOC architecture, and variation thereof in the form of an SPHRAM. Here, we describe briefly the SPHOC architecture, shown schematically in figure 1. First, rXs number of images are stored in each spot of the HMU via two-dimensional angular multiplexing, r being the number of horizontally multiplexed images, and s that of vertically multiplexed images. The process starts by expanding the collimated beam from a 20 mW solid-state green laser, for example, in order to match the size of the spatial light modulator (SLM). The target image is gathered, for example, by a camera or an SAR (synthetic aperture radar). Alternatively, the target could represent an object-to-image data map, which requires a much smaller amount of information to represent the image. A copy of the image is sent to the control computer for recording, and another copy is sent directly to the SLM via a high-speed data bus. The beam reflected from the face of the SLM carries this image. This reflected beam is now passed through the IFBR (Image Flattening Beam Reducer), which is a combination of two lenses. It reduces the image size by the ratio of the focal lengths of the two lenses, and projects a very slowly diverging version of the SLM image at the face of the next element: the HDMX (Holographic Demultiplexer/Multiplexer). The HDMX is a cloning device that produces nXm copies (which is the number of spatial locations on the HMU) of the input image, in as many angular directions. Such a device can be constructed simply by writing nXm plain wave holograms over the entire volume.

The output beams from the HDMX are now passed through an element termed the HR: the Holographic Redirector. This role of this device is to redirect the output beam from the HMDX into nXm images propagating parallel to the axis. The nXm identical copies of flattened

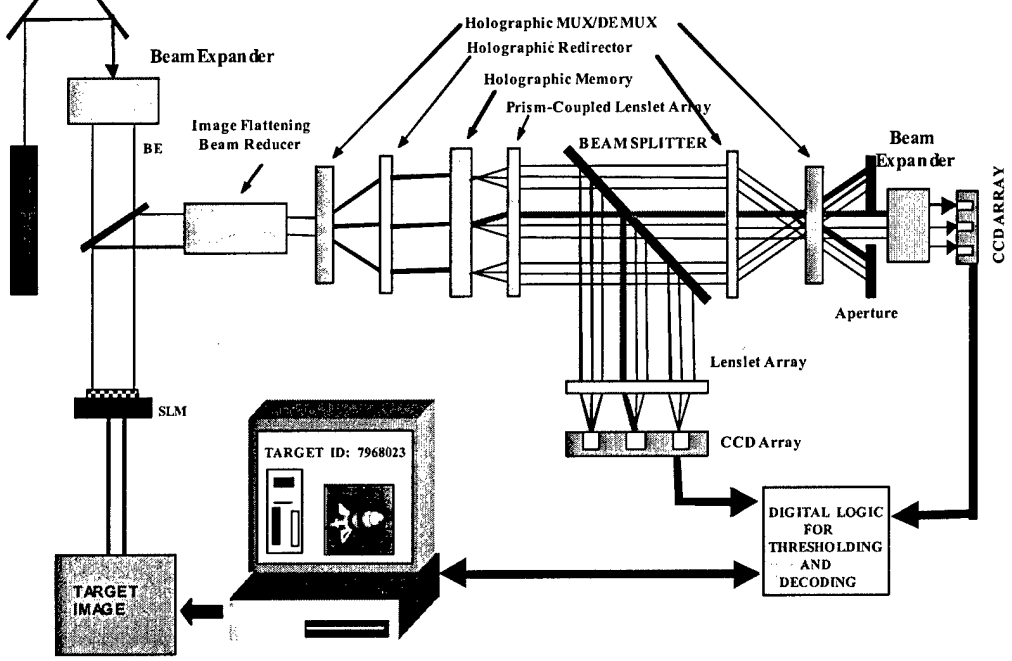

Figure 1: Schematic illustration of the Super Parallel Holographic Optical Correlator, SPHOC, which realizes a single-query process for searching through all the images stored in all the spatially distinct locations simultaneously

images now impinge on the HMU, one at each spatial location. If the image matches one in one of these locations, a correlation diffracted beam will emanate from that location in a particular angle. Here, we show all such diffraction beams (in one dimension, for simplicity of drawing), keeping in mind that only one of these beams (shown by the red/bold line) will be produced for a given image. The goal of the rest of the architecture is to identify (a) the spatial location, and (b) the angle the beam corresponds to. These two pieces of information will identify uniquely which image we have matched.

The beams coming out of the HMU need to be collimated in the direction normal to the HMU. This can be achieved via the use of a prism-coupled lenslet array (PCLA). The PCLA consists of two stages. The first stage is a simple, homogeneous, macroscopic lens array (HMLA), each of which has a diameter as big as the corresponding storage location of the HMU. The HMLA is to be positioned abutting the HMU. The second stage of the PCLA is a microscopic, inhomogeneous array of diffractive optic elements (IADOE), each of which consists of a prism, a lens, and a phase-shifter, all in series. The IADOE will be placed at the focal plane of the HMLA. By "inhomogenous" we mean that each set of these prism-lens-phaseshifter combination will have unique characteristics corresponding to its location. To understand how this would work, consider a particular HMLA element. The different plane wave (in practice, Gaussian) correlation beams generated from the HMU area in front of it will impinge on the HMLA element at different angles. As such, they will all focus on the plane of the IADOE. The phase front of each of these beams will have three factors: a constant phase shift, a linearly varying phase shift, and a quadratic phase shift. The quadratic phase shift will be the same for each of these beams; however, the constant phase shift and the linearly-varying phaseshifts will depend on the angle at which these beams were incident on the HMLA element. For the rest of the archiotecture to work, we would like each of these beams to emerge in parallel, with a Rayleigh length large enough to accommodate the rest of the elements to follow. The individual elements of the IADOE will be designed to compensate for these varying phase factors, so that after exiting the IADOE, all the beams appear to be essentially identical, expect for a translational shift. The lens in the IADOE will be used to collimate each beam , the prism (in the IADOE) will be used to compensate for the linearly varying phase shift, and the phase-shifter (in the IADOE) will be used to compensate for the constant phase shift.

The beams emerging from the PCLA are now split into two components by a beam splitter. One component goes through another lenslet array, thus getting refocused, onto an nXm array of CCD elements (CCDA). Identifying the detector that sees the highest signal yield the information about which spatial location the matching-image is in. In practical situations, the location-finder array may suffer from low signal-to-background contrast (STBC). However, with a suitably chosen signal integration time and a threshold value, it should still be possible to identify the location with any desirable degree of certainty. Alternatively, (or in addition,) the STBC can be enhanced by adding an array of MEMS based reflectors (controlled by the angle-indicator array, as described in the next section), followed by a low-pass spatial filter.

The other output of the beam splitter goes through another HR (Holographic Redirector). The HR simply redirects all the incident batches to a central point, without focusing the beams coming from the same spot with respect to one another, as shown. These beams are now passed through another HMDX, which is identical to the one used at the input, but now operating in reverse. However, the reverse operation has the potential problem that additional beam patterns (weaker than the one generated along the axis) will also be produced. A simple aperture can be

used to eliminated these unwanted spots. After the filter, we use a beam expander to match the size of the second CCD array, which contains rXs number of elements, corresponding to the number of angles used in the two-dimensional angular multiplexing during the writing stage. The element of the CCD that sees the brightest signal yields the information about the angle of the matched image. Data gathered from the detector array and the CCD array, properly thresholded, can be sent through a digital logic circuit to yield the absolute identity of the image we have matched.

DEMONSTRATING THE CONCEPT OF SPHOC:

Thick holograms have the ability to store multiple images (multiplex) in the same volume. The images can be multiplexed in several ways. Figure 2 demonstrates a technique known as angle multiplexing. The holograms are written by exposing the substrate with the image beam and a reference beam at a specific angle (Figure 2(a.)). A second image is then written with the reference beam positioned at a different angle (Figure 2(b.)). In this manner, thousands of images can be stored (Figure 2(c.)). The images are searched by illuminating the sample with a query image (Figure 2(d.)). If the image matches with a stored image, a diffracted beam emerges from the back of the sample. The direction of this beam indicates *which* image has matched. Therefore, *all of the images are searched simultaneously*.

Figure 3 displays images taken directly from the spatial light modulator (SLM) as well as images that were read from the HMU. The images are read from the HMU by illuminating the sample with the appropriately angled reference beam. A Cohu CCD camera was used to capture the images, and transferred to the computer using a frame-grabbing software. The columns marked "SLM IMAGE" shows images that are produced directly by the SLM, and captured by the CCD camera. The columns marked "HOLOGRAPHIC IMAGE" show images that were read out from the holograms, and then captured by the same CCD camera

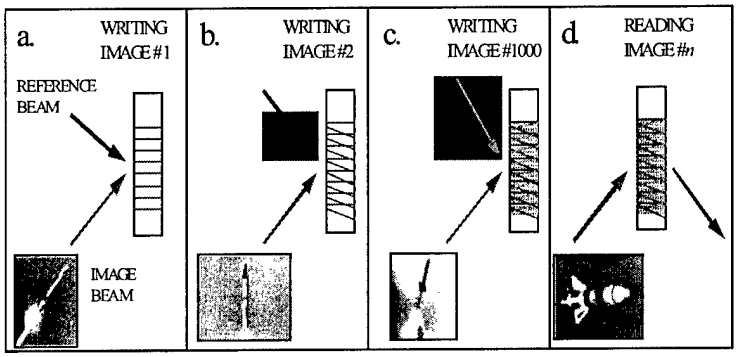

Figure 2.. Angle-multiplexed holographic image storage

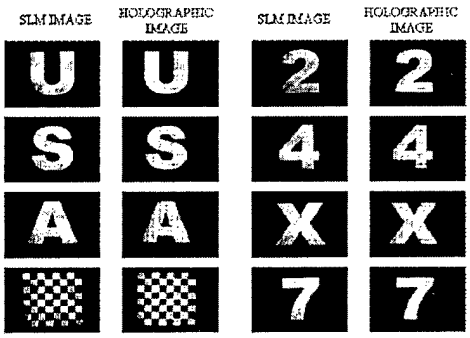

Figure 3: Sample images stored and recalled from the HMU.

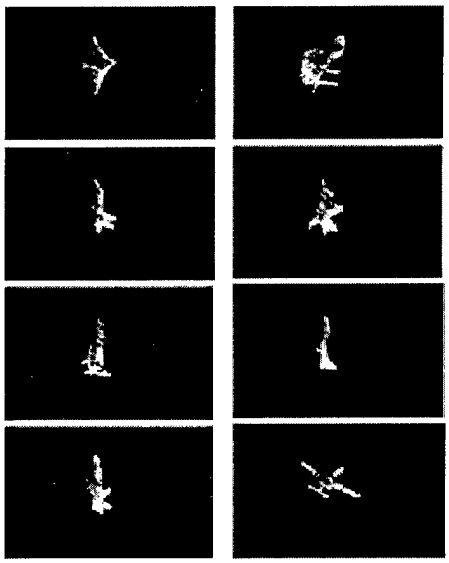

Figure 4. Eight images stored in one spatial location of a HMU unit. Each image was produced by illuminating the hologram with a plane-wave beam at the appropriate angle.

As can be seen, reasonably high-quality images were successfully stored in the PDA (photopolymer with diffusion amplification) material used for this project. The PDA material was invented originally at the Vavilov State Optical Institute (VSOI)in St. Petersburg, Russia, and its optical quality was enhanced further through collaborative work carried out between VSOI, the group of the PI, and the Laser Photonics Technology (LPT) of Amherst, NY. We can now produce this material, in virtually any custom size and shape, in our laboratory at NWU. Furthermore, LPT markets a variant of this material under the trade name of Memplex™. These holograms represent the best quality holographic images we have recorded to date. In order to achieve these results, we had to make several improvements to our setup, including robust vibration isolation, and switching from a rather unstable Ar^+ laser to the super-stable Verdi laser. Figure 4 shows another set of images stored in a single location of an HMU via angular multiplexing.

Using the same exposure and curing parameters which had previously resulted in high quality stored holographic images in the HMU, we created an HMU with three spatial locations by translating the sample in one dimension. The memory cells were placed 0.25" apart in order to avoid cross-talk between the cells. The contents of each cell were verified by illuminating the sample with reference beams and observing the holographically re-generated images. This was a key step in verifying the scalable nature of the SPHOC architecture. Following our successful writing of a HMU unit, we next attempted to correlate the stored images with query images.

In order to facilitate good spatial alignment of the HMU with the query beam, new stored images were composed. The images consisted of a three bladed "fan" that is rotated by 15 degrees with respect to the preceding image. In this way there should be no spatial overlap between the test images. An example image is shown in Figure 5. Using this new design another HMU unit was written using the same exposure and cure parameters used to produce the previous sample. We then tested the sample to insure that the holographic images had been stored. We next precisely aligned the sample with the original SLM image while observing the diffracted rays that emerged from the sample. The correlation occurs as follows: when the image projected on the sample matches one of the stored images a plane wave emerges in a specific direction. We collected all of the plane or diffracted waves with a large lens which Fourier transforms the unique angles into unique spatial locations. In this way the matching image can be determined by observing the diffraction spot intensity. Figure 9 summarizes the results of this correlation study. The images in Figure 6 represent the query image projected onto the HMU. Column II displays experimental images of the diffraction spots, and Column III. displays quantitative intensity measurements taken along the entire row of spots. As can be seen from the data, the correlation shows strong peaks with signal to noise ratios on the order of 150. This data validates the ability of the thick holographic correlator to discriminate images clearly.

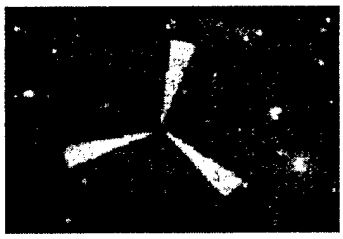

Figure 5: An example of the type of images used for demonstrating efficient correlation. This image was read from the HMU.

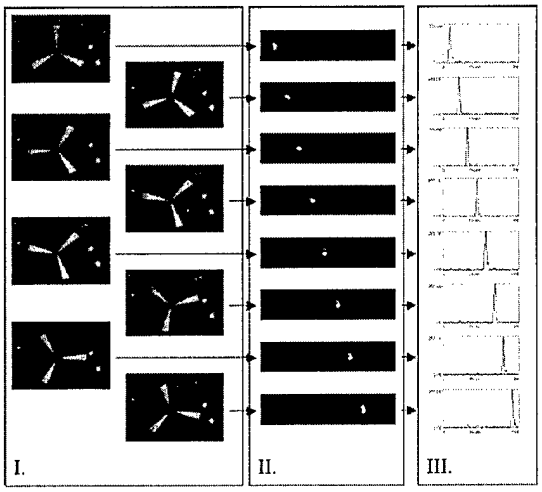

Figure 6. Demonstration of HMU image correlation

In order to demonstrate parallel image correlation, the query image was directed through a 1x3 HMDX or "splitter". This holographic optical element produces three copies of the incident image. The original SLM image as well as the resulting three projected images are displayed in Figure 7. The HMDX allows the query image to be projected simultaneously on every memory cell. In order to test each optical element, the split images were then projected onto the three-cell HMU with the use of mirrors. This provided us with the flexibility to direct each beam individually, making query-beam/HMU alignment slightly easier. The diffracted beams generated by the HMU were then collected by a lenslet array (shown in fig 8) and projected onto a CCD camera for quantitative intensity data. A schematic of this set-up is included in Figure 9.

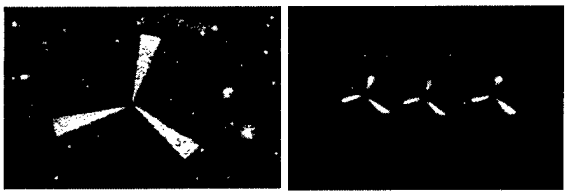

Figure 7. Image on the left is the SLM generated test image. On the right is an experimental image of the output of the 1x3 HMDX.

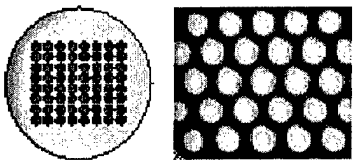

Figure 8. Schematic illustration and the image formes by a commerically available 8X8 lenslet array, housed in a circular substrate.

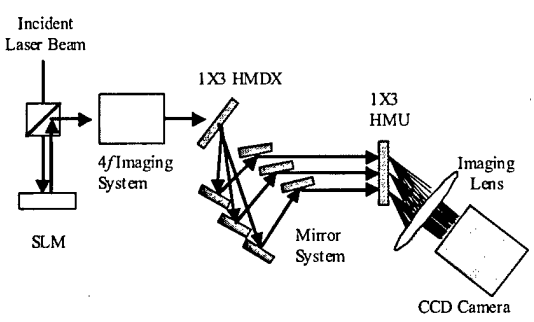

Figure 9. Schematic of correlation set-up

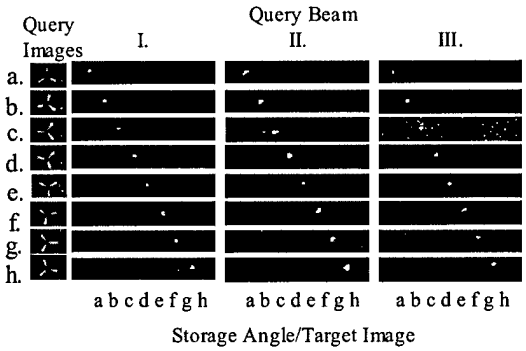

Figure 10. Correlation data from three multiplexed query images

The collected data is displayed in Figure 10. Each column represents output from each HMU memory cell. The images in the far-left column represent the query images presented to the HMU unit. The same images were stored in the HMU. The images in columns I, II, and III display the CCD images of the diffracted beams that emerged from the HMU when each of the query beams (I, II, and III) were directed onto the HMU. The lateral position of the bright spots (a, b, c...) indicates which of the stored images has matched with the query image. As the data in Figure 10 shows, the HMU is providing a clear indication of which of the stored image the queried image represents. The signal to noise ratio of this data is quite good, given the low resolution of our SLM.

The next step would be to extend this architecture to two dimensions. To this end, we have constructed and demonstrated a 1X9 HMDX, with the nine output images arranged in a symmetric 3X3 configuration. The function of this HMDX is illustrated in figure 11, with one of the fan images as a test input. As can be seen, the images are split as expected, without any significant distortions.

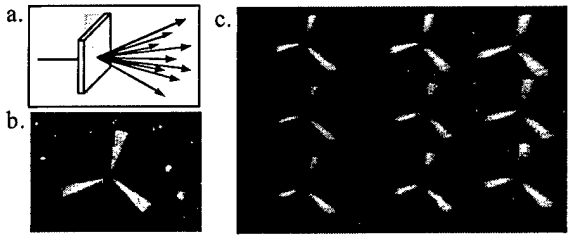

Figure 11. Demonstration of holographic multiplexer/demultiplexer (HMDX); (a) schematic of the 3X3 HMDX, (b) SLM image that was input to the HMDX, and (c) CCD capture of the nine resulting images

SUPER-PARALLEL HOLGRAPHIC RANDOM ACCESS MEMORY:

For a practical image recognition and tracking system (IRTS), it is useful to have a high-speed random access memory (RAM) to complement the SPHOC. However, the speed of a conventional RAM, which accesses data serially, is too slow for this application. Here, we show how a super-fast RAM can be realized by simply operating the SPHOC in reverse. Called the **super-parallel holographic random access memory (SPHRAM)**, this device and the SPHOC can be operated alternately using essentially the same hardware, and potentially the same data base.

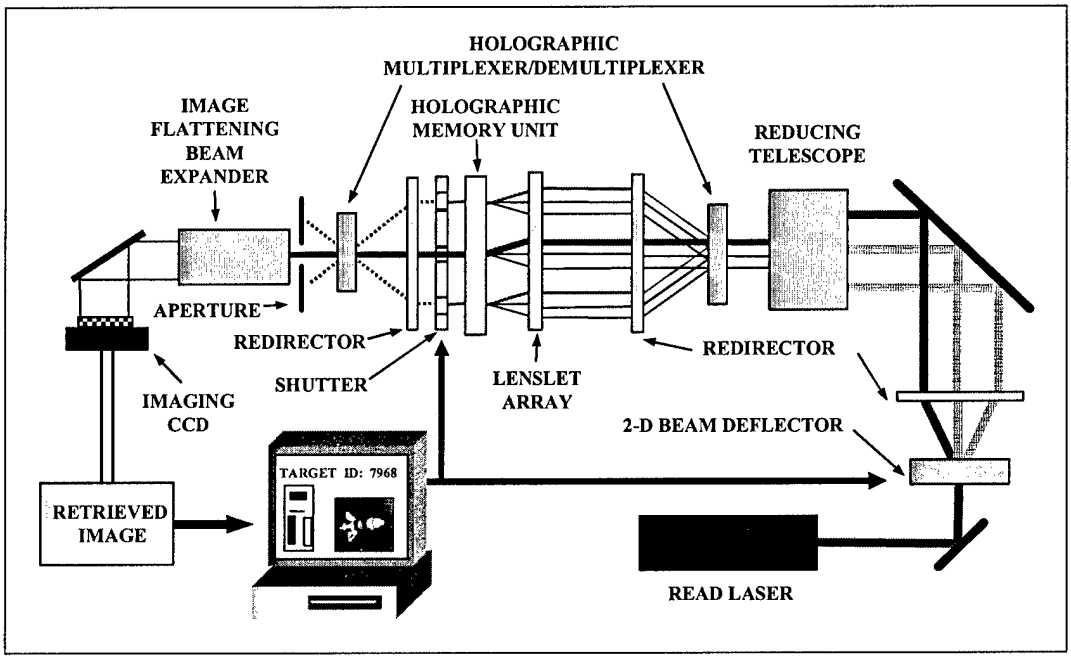

Figure 12. Schematic illustration of the Super-Parallel Holographic RAM (SPHRAM) architecture

The basic idea of the SPHRAM is illustrated in Figure 12. As stated above, the functioning of this device is similar to an SPHOC operated in reverse. Briefly, the holographic memory unit (HMU) is recorded with the database of interest, using multiple spatial locations, each of which contains a set of images that are angularly multiplexing in two dimensions. When operating the RAM, the user enters as coordinates the spatial position and the angle of storage of the image of interest. The position coordinate is used to open the corresponding element of a shutter array. The number of elements in the shutter array is the same as the number of spatial locations in the HMU, and the locations are matched. Shutter arrays of this type are available commercially, with individually addressable ferroelectric liquid crystals, for example, with a very fast switching time. The extinction ratio of these shutters can be as high as 10^5; cascading a pair of shutters can be used to achieve an extinction ratio of 10^{10}.

The angular coordinate for the image is sent to a beam deflector (e.g., using a pair of acousto-optic or electro-optic deflectors), which orients the read beam at the desired angle, which in turn is translated to a specific position by the redirector. (Alternatively, one could

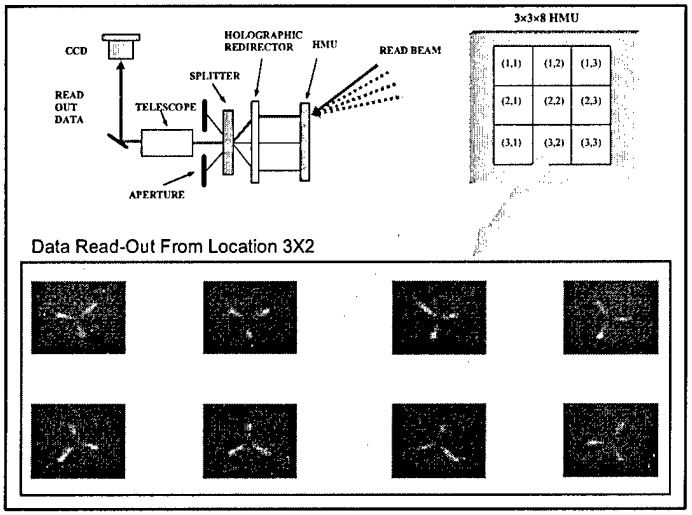

Figure 13: Examples of data pages retrieved through a simplified version of the SPHRAM architecture, using a pair of galvo-mounted mirrors for deflections

simply use an SLM, but it would reduce the amount of light available for read-out). The combination of the reducing telescope, the multiplexer, the redirector, and the lenslet array (in practice, the PCLA described above) produces a copy of the read beam simultaneously at each of the locations; this is the key feature of the SPHRAM. As such, the image stored at this angle will be recalled from each location. The shutter array will block all but one of these images, and the redirector and the demultiplexer will send the wanted image to the CCD camera.

We have recently demonstrated the feasibility of one part of the concept here, by using a pair of galvo-mounted mirrors for deflections. The geometry used by us for the demonstration is shown in figure 13. For the database, we used an existing HMU which has 9 locations, in a 3X3 arrangement, each location containing 8 images multiplexed angularly. The redirectors and the

splitter (multiplexer) used are the same as the ones created before for demonstrating the SPHOC architecture. The bottom of the figure shows a typical set of data retrieved using this setup.

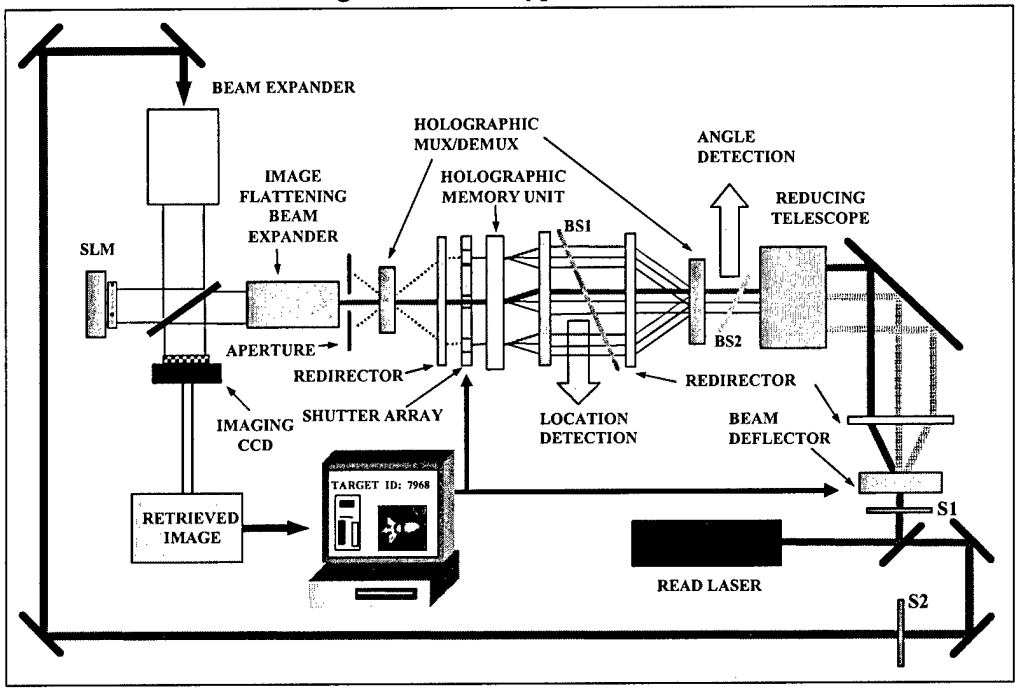

Figure 14: Schematic illustration of an architecture that can be used as either an SPHOC or an SPHRAM

Similar data were also retrieved from the other locations (not shown).

Note that a simple modification of this architecture will allow one to operate the same system as the SPHOC as well. This is illustrated in figure 14. During the operation as an SPHOC, all the elements of the shutter array are open, shutter S1 is closed, and shutter S2 is open. Beams reflected by the beam splitter BS1 is used for location detection, and the beams reflected by the beam splitter BS2 is used for angle detection. During the operation as an SPHRAM, S1 is opened, S2 is closed, and the elements of the shutter array is opened selectively according to the address of the data page to be retrieved.

ARCHITECTURAL CHALLENGES ASSOCIATED WITH THE SPHOC AND THE SPHRAM, AND THE PROPOSED SOLUTION: BEAM PROPAGATION ANALYSIS OF THE SPHOC GEOMETRY

One of the main problems associated with the SPHOC/SPHRAM architecture is that of beam collimation after the HMU. The diffraction from the holograms recorded at large angles propagate at an angle with respect to the optic axis of the system. These, when collimated using one of the lenses of the HMLA (homogeneous, macroscopic lenslet array), do not propagate parallel to the optic axis, thus creating a problem in the detector plane. As discussed above (see the two paragraphs following figure 1), this problem can be solved by adding the PCLA, to be placed at the focal plane of the HMLA. Here, we discuss these issues explicitly, using a model where the correlation beam produced is a plane wave. For a real system, this analysis has to be augmented, using FDTD (finite division time domain) techniques, by the facts that (a) the

correlation spots would be Gaussian in nature, and (b) the exact shape of the correlation spots would depend on the thick-holographic correlation process. The augmented analysis would be one of the tasks carried out under this project. Following the simplified beam propagation analysis of the system, we present the lithographic design of the prism-coupled lenslet array (PCLA) that we propose to make at Northwestern University under this project proposed here.

PROPAGATION ANALYSIS FOR THE BEAM PATH AFTER THE HMU

In order to obtain a successful detection of a match of any given HMU image, the SPHOC architecture must be able to collimate and direct every possible correlation beam towards the detector array. For a large capacity HMU, there will be many angles and thus the possible correlation beams will overlap to a large extent (Fig 15). In order to resolve each beam, a lens (i.e., an element of the HMLA) directly following the HMU can be used to focus each angled beam to a different location in the focal plane. However, the beams will still be traveling at angles to the optic axis, so redirection and collimation is necessary.

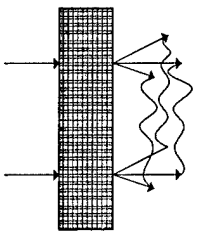

Figure 15a: Overlapping Correlation Beams

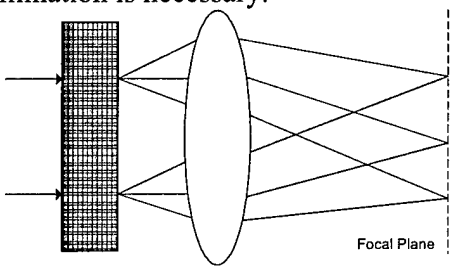

Figure 15b: Lens to separate beams

We propose to use the prism-coupled lenslet array (PCLA) described above (see the two paragraphs following figure 1) a short distance after the focal plane of this initial lens. This will redirect and collimate the beams as well as de-magnify the beams by the ratio of the focal lengths of the lens chosen. Here we use a simple method to determine the proper choice of parameters to ensure collimation and redirection parallel to the optic axis of the system.

Consider the case of a single correlation beam traveling at an angle θ with respect to the optic axis z. This beam will enter the initial lens and will be offset by a certain amount in the focal plane (Fig 16a).

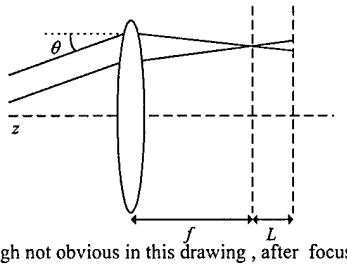

Figure 16a: Single Correlation Beam. Although not obvious in this drawing , after focusing, the beam will travel at an angle with respect to the optic axis, due to the linearly varying phase shift imparted, the amount of this being proportional to the distance of the incidence spot away from the center of the lens.

Although this picture is accurate, a more useful way to view this is to consider a shifted optic axis z' (Fig 16b), which shows explicitly that a beam incident on a lens at a position x_0 away from the center sees a phase shift corresponding to that of a lens center around the point of

incidence, and a prism, the gradient of which is proportional to x_o. Specifically, the following phase transformation will be applied to the beam:

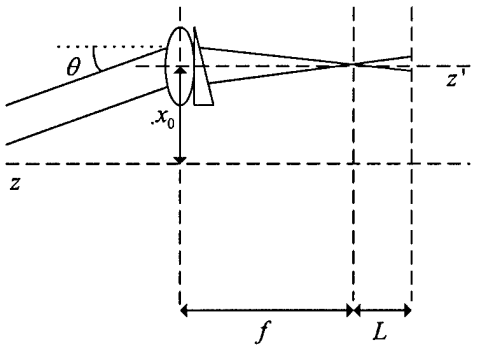

Figure 16b: Lens and Prism transformation

$$t_{lens}(x) = \exp\left(-i\frac{k}{2f}(x+x_0)^2\right) = \exp\left(-i\frac{k}{2f}x^2\right)\exp\left(-i\frac{k}{2f}2x_0x\right)\exp\left(-i\frac{k}{2f}x_0^2\right)$$

Thus this beam is affected by a quadratic phase, which focuses the beam, by a linear phase, which redirects the beam, and by a constant phase, which we make note of but disregard for now (this factor can also be compensated for in the PCLA, as discussed before).

We can express a plane wave traveling at angle θ by $U = \exp(i2\pi\upsilon_0 x)$ where $\upsilon_0 = \sin\theta/\lambda$. Therefore, the field directly after the lens-prism combination is:

$$U_{after} = \exp\left(i2\pi\left(\upsilon_0 - \frac{k\,x_0}{2\pi f}\right)x\right)\exp\left(-i\frac{k}{2f}x^2\right)$$

We use the Fresnel integral under the paraxial approximation to determine the field at z=f and z=f+L:

$$U_{z=f} = \exp\left(i\frac{k}{2f}x'^2\right)\int_{-\infty}^{\infty}\exp\left(i2\pi\upsilon_0 x - i\frac{k}{2f}2x_0x - i\frac{k}{2f}x^2 + i\frac{k}{2f}x^2 - j2\pi f'x\right)dx$$

where x' is the coordinate in the **z=f** plane, x is the coordinate in the **z=0** (initial lens) plane, and $f' = x'/\lambda f$. Again we have noted but disregarded the constant phase terms. Evaluating this integral gives us the expression for the field at **z=f**:

$$U_{z=f} = \exp\left(i\frac{k}{2f}x'^2\right)\delta\left(\frac{x'}{\lambda f} - \left(\upsilon_0 - \frac{kx_0}{2\pi f}\right)\right)$$

We can now use the Fresnel integral a second time to propagate this field to **z=f+L**:

$$U_{z=f+L} = \exp\left(i\frac{k}{2L}\right)\int_{-\infty}^{\infty}\exp\left(i\frac{k}{2f}x'^2\right)\delta\left(\frac{x'}{\lambda f}-\left(\upsilon_0-\frac{kx_0}{2\pi f}\right)\right)\exp\left(i\frac{k}{2f}x'^2-j2\pi f''x'\right)dx'$$

In this expression x'' is the coordinate in the **z=f+L** plane. Evaluating this integral gives us our final expression for the field in the **z=f+L** plane. We note that it has a quadratic phase factor as expected by the focusing action of the lens, and that the field is traveling tilted with respect to the optic axis.

$$U_{z=f+L} = \exp\left(i\frac{k}{2L}x^2\right)\exp\left(-i2\pi\frac{f}{L}\left(\upsilon_0-\frac{x_0}{\lambda f}\right)x\right)$$

This yields the information on the focal length of the lens (in the PCLA) we will need to cancel the quadratic phase term, as well as the angle of the prism (also in the PCLA, juxtaposed to the lens) needed to cancel the linear phase term, thus producing a plane wave traveling parallel to the optic axis. By keeping track of all the constant phase terms added by the prisms, lenses, and free-space propagation, we can also add a phase plate to the PCLA. The final array will consist of a quadratic phase correction, a linear phase correction, and a phase-compensator plate, yielding at its output collimated plane waves traveling along the optic axis, in phase, as required by the SPHOC/SPHRAM architecture..

Assuming a 3mm beam diameter entering the first lens (f=1cm) and a desired diameter of $300\,\mu m$, the second lens will have a focal length of 2mm and the output beam will have a Rayleigh range of approximately 53 cm at 532nm. Such a long Rayleigh range is more than adequate for the architecture of the SPHOC and the SPHRAM.

LITHOGRAPHIC DESIGN AND CONSTRUCTION OF THE PRISM-COUPLED LENSLET ARRAY AND OTHER CHALLENGING COMPONENTS:

The beam path from the HMU to the prism-coupled lenslet array is shown in fig. 17 below (the unfilled dots in the focal plane are meant to all lie in plane perpendicular to the propagation axis, and each dot represents an element of the PCLA). As mentioned earliar, the HMU generates rXs diffracted beams from each of its nXm locations. For simplicity, we show an off-axis propagation here. All the diffracted beams are focused in the focal plane of the lens (which is an element of the HMLA). The beams then propagate further as per their corresponding divergence. Each of these beams is then collected by an element of the prism-coupled lenslet array (PCLA), which collimates the beam along the optic axis of the system. As illustrated in detail above, this PCLA is to be custom-designed so that: (a) each element of the array has a prism with a unique deflection angle corresponding to the linearly varying phase shift experienced by the input beam, (b) the lenses in the array have the same focal length, and they collimate the incident beams along the optic axis, and (c) each element provides a unique and constant phase shift factor.

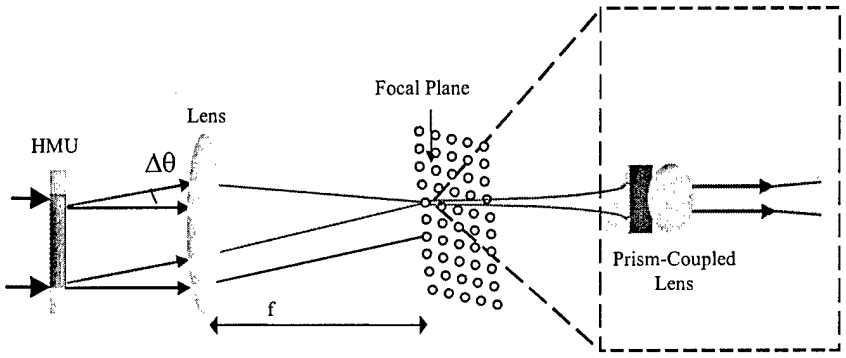

Figure 17: Beam Propagation from HMU to the Proposed Prism-Coupled Lenslet Array

Specifically, one can fabricate the focusing lens along with the prism-coupled lenslet array using a silicon bench. This would enable an easy pre-fabricated alignment of each individual element in the array. The following figure (figure 18) depicts one such assembly. The basic construction of prism-coupled lenslet array is based on very strong graded-refractive-index (GRIN) structure to achieve focusing along the optic axis of the SPHOC system, which will be vertical to the Silicon bench on which we will fabricate the whole assembly. Phase correction in this direction can be achieved by refractive index profile as shown in Fig 19a. In the other direction (horizontal to Si bench), focusing and phase correction are achieved by physical curved surfaces (lens plus prism) as shown in Fig. 19(b).

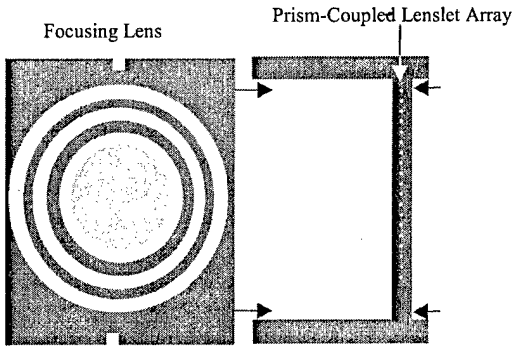

Figure 18: Assembly showing the focusing lens along with the prism-coupled lenslet array

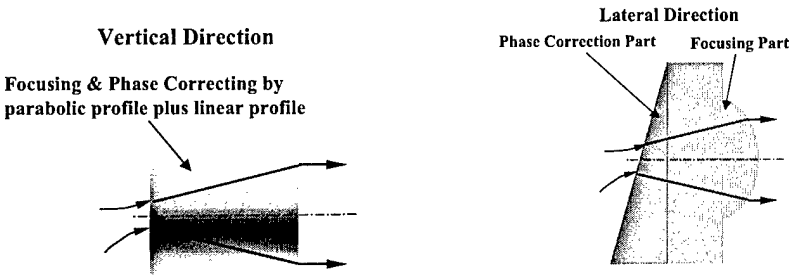

Fig 19 Precision lens outline: (a) vertical focusing and phase correction by multilayer structure. (b) Lateral focusing and phase correction by physical surface profile

Suppose refractive index at the center of the GRIN is n_o and the refractive index on the side is n_R, the effective refractive index difference is defined by $dn = \sqrt{n_0^2 - n_R^2}$. According to GRIN lens formula, the numerical aperture NA is about the same value as *dn*. The spot size σ (FWHM) is $0.6\lambda/dn$. One limitation of the conventional GRIN lens is that high NA cannot be achieved, as the graded refractive index profile is achieved via material diffusion technique. Such technique cannot achieve large difference in refractive indices between the lens center and side. Another limitation is the refractive index profile cannot be arbitrary. The superlens is capable of correcting for beam's spatial aberration and astigmatism. It is a powerful precision lens that can be made directly on silicon bench in large number with each lens capable of performing individual complex beam profile transformation.

GRIN lens fabrication methods makes use of By inter-spacing *multiple-layer thin films of two materials with drastic difference in refractive index to achieve a highly controllable refractive index variation.* one high refractive index material with another low refractive index material, we can get effective refractive index of any value in between. The principle of this technique is shown in fig 20. When mixing thin layer of two different refractive index materials, the effective refractive index of the mixed section can be calculated as:

$$n_{eff} = \frac{n_1 L_1 + n_2 L_2}{L_1 + L_2}$$

where n_1 is the higher refractive index, n_2 is the lower refractive index, L_1 is the thickness of the higher refractive index material and L_2 is the thickness of the lower refractive index material.

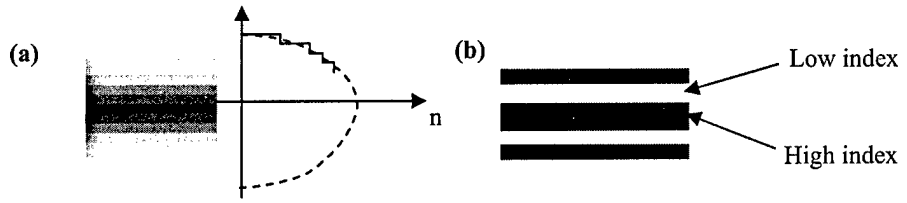

Fig. 20 (a) Two-material layered structure with parabolic graded refractive index profile; (b) Mix two materials to get the varying effective index to achieve desired index.

Using SiO_2/TiO_2, a refractive index variation of 1.5 to 2.4 can be achieved (Fig. 21(a)). In Fig. 21(b) below, one can show the strong focusing capability of this dual material structure by Finite Difference Time Domain (FDTD) simulation.

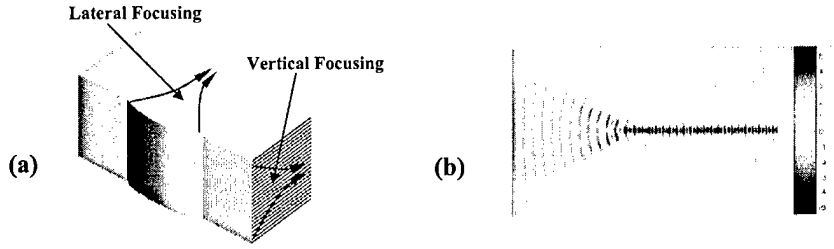

Fig. 21 (a) 3D Lens structure. (b) FDTD simulation of precision lens in vertical direction, with output to 150nm channel waveguide

The dual material structure is able to provide any refractive index profile, such as parabolic graded profile plus linear graded profile. The parabolic profile will provide focusing or collimating and the linear profile will provide phase correction as shown in Fig. 19(a).

In lateral direction, focusing and phase correction are achieved by physical curved surfaces, which can be any shape because it is only defined by photolithographic mask. As shown in Fig. 22, the lens part is providing focusing and the prism part provides phase correction. To produce the parallel beam OCM, different phase correction (or angular transformation) as shown in (a), (b), (c) are needed at different FP focused points (see Fig. 22(d)). Using superlens, these slightly different lenses can be fabricated in a single run of fabrication.

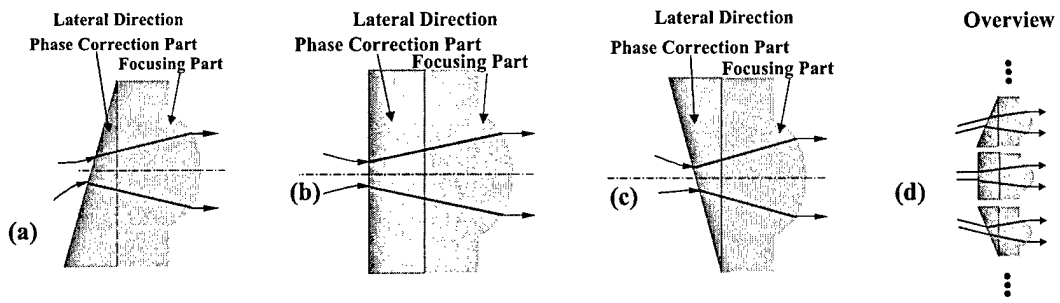

Fig. 22. Lateral focusing plus different phase correction (a, b, c, d).

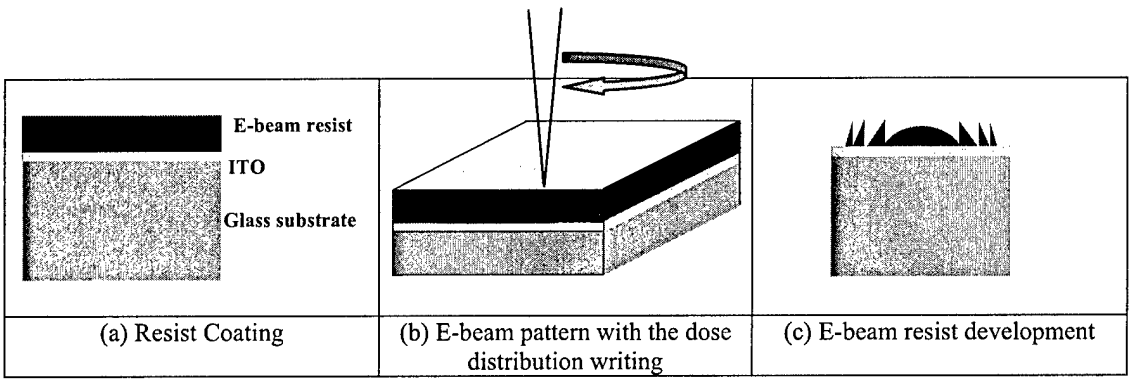

Figure 23. Procedure of the electron-beam writing fabrication of Fresnel lens

The Fresnel lens can be fabricated using e-beam lithography. The electron-beam writing procedure of fabrication Fresenl lens is shown in Fig. 23. First, an electron-beam resist is spin-coated on a glass substrate covered with a transparent conductive layer of ITO, which is necessary to avoid electrical charge buildup during the writing. In order to increase the diffraction efficiency of Fresnel lens, a blazed Fresnel grating is required in the process. The initial resist layer should be slightly thicker than the final thickness after having been developed. We can use PMMA (positive type) or CMS (negative type) e-beam resist, where CMS stands for chloromethylated polystyrene. The final thickness is determined by working wavelength and E-beam resist refractive index. Our system working wavelength is λ=0.532μm and E-beam resist refractive index n=1.49 (PMMA). The final thickness is estimated to be about $T = \lambda/(n-1) = 1.08\mu m$. Second, the blazed profile can be formed by a suitably chosen electron-dose distribution because the etching rate of the resist will depend on the electron dose. The electron-dose versus etch-depth relationship is obtained from a cross-sectional scanning-electron-microscope photograph of test sample that has been drawn by linearly changing the dose. After getting the electron-dose versus etch-depth relationship, one can scan the sample at different locations of the Fresnel for a different predetermined time until the specified dose is given to obtain the blazed grating shape shown in Fig. 23c. Third, after exposure the sample is carefully developed in 1:1 solution of isopropyl alcohol and methyl isobutyl ketone. The development of the resist would achieve the desired relief structure.

References: Primary

1. P.W. Shor, "Algorithms for quantum computation: discrete logarithms and factoring," in Proceedings, 35th Annual Symposium on Foundations of Computer Science, IEEE Press, Los Alamitos, CA 1994.
2. L.K. Grover, "Quantum Mechanics helps in searching for a needle in a haystack." Phys. Rev. Lett. 79(2):325, 1997.
3. M.Scully and S. Zubairy, "Quantum search protocol for an atomic array," Phys. Rev. A, 64, 022304 (2001)
4. M.S. Shahriar, M. Kleinschmit, J. Donoghue, W. Weathers, and R. Tripathi, "Demonstration of a Super Parallel Holographic Optical Correlator for Ultrafast Database Search," Postdeadline paper, Conference on Lasers and Electro-Optics, 2002.
5. M.S. Shahriar, R. Tripathi, M. Kleinschmit, J. Donoghue, W. Weathers, M. Huq, J.T. Shen, "Super-Parallel Holographic Optical Correlator for Ultrafast Database Search", *Opt. Letts. **28**, pp. 525-527* (2003)
6. "Holographic Correlation Improves on DSP by Six Orders of Magnitude," by Hassaun A. Jones-Bey, *The Laser Focus World*, July 2002.
7. .N. Collins, *Optical Pattern Recognition Using Holographic Techniques,* (Addison-Wesley, Reading, Ma 1988).
8. M.S. Shahriar, J. Riccobono, M. Kleinschmit, and J. Shen " Coherent and Incoherent Beam Combination Using Thick Holographic Substrates" Opt. Commun., **220**, 1, pp. 75-83(2003)..
9. L. Wong, M. Bock, B. Ham, S. Shahriar, and P. Hemmer, "Ultra-High Density Optical Data Storage," in *Symposium on Electro-Optics: Present and Future*, Optical Society of America book series on *Trends in Optics and Photonics* (1998).
10. M.S. Shahriar, J. Shen, R. Tripathi, and M. Huq, "Simultaneous Operation of A Super-Parallel Holographic Optical Correlator and a Super-Parallel Holographic RAM," to appear as an invited paper for the *Special Issue* of *Optical Engineering* on *Trends in Pattern Recognition Algorithms, Architectures, and Devices*, 2004

Additional References : Holographic Optical Computing

1. L. Wong, M. Bock, B. Ham, S. Shahriar, and P. Hemmer, "Ultra-High Density Optical Data Storage," in *Symposium on Electro-Optics: Present and Future*, Optical Society of America book series on *Trends in Optics and Photonics* (1998).
2. J.E. Ludman, J. Riccobono, N. Reinhand, Y. Korzinin, I. Semenova, S. Shahriar, "Nonspatial filter for laser beams," 8th Laser Optics Conference, 27 June – 1 July 1995, St. Petersburg, Russia, *Proceedings SPIE.*
3. J. Ludman, J. Riccobono, N. Reinhand, I. Semenova, Y. Korzinin, and S. Shahriar, "Holographic Nonspatial Filter," *SPIE Proceedings*, 2532, 481-490 (1995).
4. J. Ludman, J. Riccobono, N. Reinhand, I. Semenova, Y. Korzinin, S. Shahriar, J. Caulfield, J. Fournier, P. Hemmer, "Very Thick Holographic Nonspatial Filtering of Laser Beams," Optical Engineering 36, 6 (1997).
5. J. Ludman, J. Riccobono, N. Reinhand, Y. Korzinin, I. Semenova, and S. Shahriar "Two Dimensional Holographic Nonspatial Filtering," Practical Holography, Feb 1996, SPIE IS&T Conference, San José, CA.
6. P.R. Hemmer, M.S. Shahriar, M.K. Kim, K.Z. Cheng and J. Kierstead, "Time Domain Optical Data Storage using Raman Coherent Population Trapping," *Opt. Letts.* **19**, 296 (1994).
7. M.S. Shahriar, L. Wong, M. Bock, J. Kierstead, P.R. Hemmer, M. Henrion, and J. Ludman, "Angle and space multiplexed holographic optical memory using thick, diffusion amplified photopolymer," the OSA Annual Meeting, 1998, Baltimore, MD.
8. P.R. Hemmer, D.P Katz, J. Donoghue, M.S.Shahriar, P. Kumar, and M. Cronin-Golomb,"Efficient, Low Intensity Optical Phase Conjugation Using Coherent Population Trapping in Sodium," Opt. Letts., 20, 982(1995).

9. T.T. Grove, E. Rousseau, X. -W. Xia, M.S. Shahriar, and P.R. Hemmer, "Efficient and Fast Optical Phase Conjugation by use of two-photon-induced gratings in the orientation of angular momentum," *Opt. Letts.* **22**, 1677(1997).
10. V.S. Sudarshanam, M. Cronin-Golomb, P.R. Hemmer, and M.S. Shahriar, "Turbulence Aberration Correction with High-Speed High-Gain Optical Phase Conjugation in Sodium Vapor," *Opt. Letts* **22,** 1141(1997).
11. B.S. Ham, M.S. Shahriar, M.K. Kim, and P.R. Hemmer, "Frequency Selective Time Domain Optical Data Storage by Electromagnetically Induced Transparency in a Rare-earth Doped Solid," *Opt. Letts.* **22,** 1849(1997).
12. D. Hsiung, X. Xia, T. Grove, S. Sudarshanam, P. Hemmer, and M.S. Shahriar, "Demonstration of a Ring Laser using a Rb Phase Conjugator as an amplifying mirror," *Opt. Commun.,* **154** (1998) 79-82.
13. V. S. Sudarshanam, M. Cronin-Golomb, P. Hemmer, and M.S. Shahriar, "Raman phase conjugate resonator for intracavity aero-optic turbulence aberration correction," *Opt. Commun.* **160**, 283 (1999).
14. M.S. Shahriar, J. Riccobono, and W. Weathers, "Holographic Beam Combiner," presented at the IEEE International Conference on Microwave and Optics, Rio De Janeiro, Brazil, August 10-14th, 1999;
15. M.S. Shahriar, J. Riccobono, and W. Weathers, "Multiwave-Mixing in a Thick Hologram with Applications to Beam Combining," submitted to *J. Opt. Soc. Of America B.*
16. "Bi-functional Chromophore for Photorefractive Applications", Yue Zhang, Christopher C. Spencer, Saswati Ghosal, Martin K. Casstevens and Ryszard Burzynski, *Appl. Phys. Lett.*, **66(3)**, 256, 1995.
17. "Photorefractive Processes in polymers and organic-inorganic glass composites", Paras N. Prasad, Maciek E. Orczyk, Bogdan Swedek, Jaroslaw J. Zieba, Chanfang Zhao, C.-Kim Park, Ryszard Burzynski, Yue Zhang, Saswati Ghosal, Martin K. Casstevens, SPIE **2527,** 231 (1995).
18. "New Copolymers for Applications as Organic LEDs", Charles W. Spangler, J.W. Thurmond, M. He, Saswati Ghosal, Yue Zhang, Martin K. Casstevens and Ryszard Burzynski, SPIE *Optical and Photonic Applications of Electroactive and Conducting Polymers,* **2528**, 46 (1995).
19. "Photorefractive Composites with High-Band-Gap Second-Order Nonlinear Optical Chromophores," Ryszard Burzynski, Yue Zhang, Saswati Ghosal, Martin K. Casstevens, *J. Appl. Phys.*, **78**, 6903 (1995).
20. "Novel Optical Composites:Second Order NLO materials and Polymeric Photorefarctive Materials For Optical Information Storage and Processing Applications", Ryszard Burzynski, Martin K. Casstevens, Yue Zhang and Saswati Ghosal, *Opt. Eng.*, **35**, 443 (1996).
21. "Photorefractive Polymers and Composite Materials," Yue Zhang, Ryszard Burzynski, Saswati Ghosal, and Martin K. Casstevens, *Adv. Mat.*, **8**, 111 (1996).
22. "Sol-Gel Processed Photorefractive Materials", Ryszard Burzynski, Saswati Ghosal, Martin K. Casstevens and Yue Zhang, *Better Ceramics Through Chemistry VII: Organic/ Inorganic Hybrid Composites, MRS Symp. Proc.*, **435**, 595 (1996)
23. "Photorefractive Composite Materials with Bi-Functional Charge Transporting Second-Order Nonlinear Optical Chromophores," Yue Zhang, Saswati Ghosal, Martin K. Casstevens, and Ryszard Burzynski, *J. Appl. Phys.*, **79**, 8920 (1996).
24. "New Application for a Well Known Molecule: PRODAN as an Attractive, Optically Second Order Nonlinear Chromophore," Jayant D. Bhawalkar, Jaroslaw Zieba, Michal Kazmierczak, Paras N. Prasad, Yue Zhang, Saswati Ghosal, Martin K. Casstevens and Ryszard Burzynski, *Nonlinear Opt.*,**16**, 95 (1996).
25. "New PVK-Based Photorefractive Polymers", Ryszard Burzynski, Saswati Ghosal, Martin K. Casstevens, Deepak N. Kumar, John F. Weibel, in *Applications of Photonic Technology 3*, R. A. Lessard, G. A. Lampropoulos, Ed., SPIE **3491**, 714 (1998).
26. "Crosslinkable Polyimides for Electrooptic Applications", Ryszard Burzynski, Saswati Ghosal, John F. Weibel, Paul M. Kurtz, Martin K. Casstevens, in *Applications of Photonic Technology 3*, R. A. Lessard, G. A. Lampropoulos, Ed., SPIE **3491**, 751 (1998).
27. "The Optical Behavior of New Dyes in Nanoporous Glasses." Martin K. Casstevens, D. N. Kumar, Saswati Ghosal, Ryszard Burzynski, C. W. Spangler, E. H. Elandaloussi, *Nonlinear Optics*, **21**, 263 (1999).
28. "Dynamic Self-Enhanced Diffraction From Written Photorefractive Gratings", Liangmin Zhao, Paras N. Prasad, Ryszard Burzynski, Huanchu Chen, Jianru Han, *J. Appl. Opt.*. , **87**, 643 (2000).
29. "New Photopolymer for Holographic Optical Storage Technology", Ryszard Burzynski, Deepak N. Kumar, Martin K. Casstevens, Dale Tyczka, Saswati Ghosal, Paul M. Kurtz, John F. Weibel, in

Applications of Photonic Technology 4, R. A. Lessard, G. A. Lampropoulos, Ed., SPIE **4087**, 741 (2000).
30. W. Gambogi, K. S. Mackara, T. Duzick, B. Hamzavy and J. Kelly, *Proc. SPIE* **2152**, (1994).
31. D. H. Whitney and R. T. Ingwall, *Proc. SPIE* **1213**, 18 (1990).
32. R. T. Ingwall, D. Waldman in *Holographic Data Storage*, H. J. Coufal, D. Psaltis, G. T. Sincerbox, Eds., Spriger, New York 2000, pp. 171-197.
33. V. L. Colvin, R. G. Larson, A. L. Harris, M. L. Schilling, *J. Appl. Phys.*, **81**, 5913-5923 (1997); L. Dhar, M. G. Schones, H. E. Katz, A. Hale, M. L. Schiling, A. L. Harris in *Holographic Data Storage*, H. J. Coufal, D. Psaltis, G. T. Sincerbox, Eds., Spriger, New York 2000, pp. 200-208.
34. T. Bieringer in *Holographic Data Storage*, H. J. Coufal, D. Psaltis, G. T. Sincerbox, Eds., Springer, New York 2000, pp. 209-228.
35. R. Burzynski, D. N. Kumar, M. K. Casstevens, D. Tyczka, S. Ghosal, P. M. Kurtz, J. F. Weibel: "New Photopolymer for Holographic Optical Storage Technology" in *Aplications of Photonic Technology 4*, R. A. Lessard, G. A. Lampropoulos, Editors, *SPIE*, **4087**, 741-753 (2000).
36. F. Mok, G. W. Burr, D. Psaltis, *Opt. Lett.*, **21**, 896 (1996).
37. M.S. Shahriar, M. Kleinschmit, J. Donoghue, W. Weathers, and R. Tripathi, "Demonstration of a Super Parallel Holographic Optical Correlator for Ultrafast Database Search," Postdeadline paper, Conference on Lasers and Electro-Optics, 2002.
38. M.S. Shahriar, M. Kleinschmit, J. Donoghue, W. Weathers, and R. Tripathi, "A Super Parallel Holographic Optical Correlator for Ultrafast Database Search," Presented at the OSA Annual Meeting, Orlando, Fl (Sept. 2002)
39. "Holographic Correlation Improves on DSP by Six Orders of Magnitude," by Hassaun A. Jones-Bey, *The Laser Focus World*, July 2002.
40. W.W. Goj, *Synthetic-Aperture Radar & Electronic Warfare*, (Artec House, NY 1992).
41. Dag. Stranneby, *Digital Signal Processing: DSP and Applications*, (Oxford, Newnes, 2001).
42. G. Barbastathis and D. Psaltis, "Volume Holographic Multiplexing Methods" in *Holographic Data Storage*, H.J. Coufal, D. Psaltis, G.T. Sincerbox eds. (Springer-Verlag, Heidelberg, 2000).
43. J.W. Goodman, *Introduction to Fourier Optics* (1996).
44. A. Vanderlugt, *IEEE Information* **1**, 139 (1964).
45. N. Collins, *Optical Pattern Recognition Using Holographic Techniques,* (Addison-Wesley, Reading, Ma 1988).
46. AV Pavlov, EI Shubnikow, "Pattern recognition by optical neural network based on the optical correlator" *Optical Memory & Neural Networks,* 2, 4, (1993).
47. G.W. Burr, C. Jefferson, H. Coufal, M. Jurich, J. Hoffnagle, R. Macfarlane, R. Shelby, "Volume holographic data storage at areal density of 250 gigapixels/in," *Opt Lett* **26** 44-446 (2001).
48. J.L. Sanford, "A one-megapixel reflective spatial light modulator system for holographic storage" *IBM J Res Dev*, **42** 411-426 (1998).
49. D. Psaltis, D. Brady, and K. Wagner, "Adaptive optical networks using photorefractive crystals" *Appl. Opt.* **27,** 1752 (1988);
50. G.W. Burr, F.H. Mok, D. Psaltis, "System metric for holographic memory systems," *Opt Lett* **21** 896-898 (1996).
51. M.S. Shahriar, R. Tripathi, M. Kleinschmit, J. Donoghue, W. Weathers, M. Huq, J.T. Shen, "Super-Parallel Holographic Optical Correlator for Ultrafast Database Search", *Opt. Letts. 28, pp. 525-527* (2003)
52. M.S. Shahriar, J. Riccobono, M. Kleinschmit, and J. Shen " Coherent and Incoherent Beam Combination Using Thick Holographic Substrates" to appear in *Opt. Commun.* (2003).
53. *"Biomolecular Electronics: Protein-Based Associative Processors and Volumetric Memories,"* Robert R. Birge, Nathan B. Gillespie, Enrique W. Izaguirre, Anakarin Kusnetzow, Albert F. Lawrence, Deepak Singh, Q. Wang Song, Edward Schmidt, Jeffrey A. Stuart, Sukeerthi Seetharaman, and Kevin J. Wise, *J. Phys. Chem. B*, **103**, 10746-10766 (1999).
54. A. Adibi, K. Buse, D. Psaltis: ""Non-volatile holographic recording in doubly-doped lithium niobate,"" Nature, vol. 393, pp. 665-668, 1998.
55. Ali Adibi, K. Buse, D. Psaltis: ""Sensitivity improvement in two-center holographic recording," Optic Letters, vol. 25, pp. 539-541, 2000.

Additional References: Lithographic Integrated Optics:

(1). Hiroaki Nakamura, Toshiharu Saiki, Hirotomo Kambe and Keiji Sawada, .FDTD simulation of tapered structure of near-field fiber probe, Computer Physics Communications, Volume 142, Issues 1-3, 15 December 2001, Pages 464-467
(2). S. T. Chu, W. P. Huang and S. K. Chaudhuri, .Simulation and analysis of waveguide based optical integrated circuits., Computer Physics Communications, Volume 68, Issues 1-3, November 1991, Pages 451-484
(3). Beom-hoan O, Se-Geun Park, Sang-Ho Rha and Jae-Seong Jeong, .Improved etching characteristics of silicon-dioxide by enhanced inductively coupled plasma., Surface and Coatings Technology, Volumes 133-134, November 2000, Pages 589-592
(4). Sun-Tae Jung, Hyung-Seung Song, Dong-Su Kim and Hyoun-Soo Kim, .Inductively coupled plasma etching of SiO2 layers for planar lightwave circuits., Thin Solid Films, Volume 341, Issues 1-2, 12 March 1999, Pages 188-191
(5). J. W. Lee, J. F. Donohue, K. D. Mackenzie, R. Westerman, D. Johnson and S. J. Pearton, .Mechanism of high density plasma processes for ion-driven etching of materials., Solid-State Electronics, Volume 43, Issue 9, September 1999, Pages 1769-1775

[SEE ATTACHMENT 1 FOR FURTHER DETAILS]

3.2 Theory Of Holographic Beam Combining With Applications To Super-Dense Wavelength Division Multiplexing And Holographic Correlators

We have developed a mathematical model of coherent and incoherent beam combination in a thick hologram. We also derive the formulae relating the read and write angles to the read and write wavelengths for the combiner. Furthermore, we present a new technique for determining the M#, and establish that the M# required for a coherent combiner is substantially less than that needed for an incoherent one. These models are of direct importance to developing key components of the SPHOC architecture described above, as well as for potential applications to super-dense WDM systems based on holographic beam combiners.

[SEE ATTACHMENT 2 FOR DETAILS]

3.3 Demonstration Of Nitrogen Vacancy Color Center In Diamond As A Viable Medium For SHB Memory

We have observed Raman-excited spin coherences in nitrogen-vacancy diamond color centers by means of nondegenerate four-wave mixing and electromagnetically induced transparency. The maximal absorption suppression was found to be 17%, which corresponds to 70% of what is possible given the random geometric orientation of the color center in diamond. This experiment demonstrate the feasibility of high-capacity, high-speed data storage via Raman type SHB process in this material.

[SEE ATTACHMENT 3 FOR DETAILS]

3.4 Demonstration Of Slowing and Stopping of a Light Pulse in a Crystal of Pr:YSO with Applications to Data Buffering and Quantum Memory

We have demonstrated ultraslow group velocities of light in an optically dense crystal of Pr:YSO. Light speeds as slow as 45 m/s were observed, corresponding to a group delay of 66 ms. Deceleration and "stopping" or trapping of the light pulse was also observed. These reductions of the group velocity are accomplished by using a sharp spectral feature in absorption and dispersion that is produced by resonance Raman excitation of a ground-state spin coherence. This process has potentially significant applications in buffering of high-bit-rate data streams in optical communication, as well as in realizing a high-fidelity quantum memory system.

[SEE ATTACHMENT 4 FOR DETAILS]

3.5 A Holographic Stokes-meter for Polarization Imaging

Polarimetric imaging[1-3] takes advantage of the fact that a given object emits and scatters light in a unique way depending on its polarimetric signature. Identifying the polarimetric signature is equivalent to identifying the scattered Stokes vector[4,5]. An active polarimetric sensor is used in applications such as target recognition, vegetation mapping, pollution monitoring, geological surveys, medical diagnostics and so on.[6-9]

Current polarization imaging systems include mechanical quarter-wave plate/linear polarizer combinations[10], photo-detectors with polarization filtering gratings etched onto the pixels, and liquid crystal variable retarders. The speed of the mechanical sensor is limited because each Stokes parameter is determined sequentially and the wave plate/polarizer combination must be re-oriented precisely between parameters. The etched photo-detector systems cannot resolve the complete Stokes vector at this time. The liquid crystal retardation is very similar to the mechanical sensor but with a liquid crystal display replacing the wave plates and polarizers. This method is still sequential and is restricted by the time it takes the display to re-orient itself, typically on the order of 100ms per scan. This limits the throughput to ~ 10 Hz. To examine the advantages of the proposed architecture and to quantify its speed, we examine each component (see Figure 1). A typical thick hologram (~1mm) has a channel bandwidth on the order of 1 nm (and an angular bandwidth of ~1 mrad), corresponding to an optical response time of ~10 ps. The signal manipulation can be accomplished with pre-calibrated field-programmable gate arrays (FPGA) or programmable logic arrays (PLA) and does not require real-time processing. These devices perform at roughly the speed of the logic gates, typically on the order of 1 ns. The detector array response time is determined in part by the desired signal to noise ratio (SNR). The SNR is proportional to $\sqrt{\eta I \tau}$, where η is the quantum efficiency, I is the intensity, and τ is the average time. For a typical SNR of 10, the response time is then given by the detector-specific parameters and the amount of light reflected by the target. It should be noted that the constraints imposed by a given SNR and the detector array are common to all of the methods discussed here. The advantage of our design is that it can determine the complete Stokes vector in parallel, so that the detector and not the sensor is the limiting factor in determining the speed of the device.

The architecture is shown in Figure 1. The incoming image is split into two copies using a beam splitter. The first beam is diffracted into two beams using two multiplexed holographic gratings. The second beam passes through a quarter-wave plate before diffracting from a similar set of multiplexed holographic gratings. The diffracted beams are projected onto four CCD arrays. Their intensities are summed with pre-determined weights to compute each component of the Stokes vector. These weighting factors are determined by using the parallel and perpendicular polarization components of diffraction to formulate the Mueller matrix that describes the transformation of the initial Stokes parameters by grating diffraction. This design takes advantage of the fact that a hologram is sensitive to the polarization of the incident light, and the weighting factors can be determined analytically by using a Mueller matrix analysis of the architecture.

For an arbitrary image pattern, the diffraction efficiencies depend also on the range of spatial frequencies. Here, we restrict our analysis to the simple case of a plane wave incidence, which can be extended easily to analyze the general case. Figure 2

illustrates the progression of the light through a thick hologram. This process is represented mathematically by a series of Mueller matrices[11,12] that describe the transformation of the input Stokes vector S_i. The Stokes vector S_{FS} of the transmitted beam through the front surface of the hologram is

$$\mathbf{S_{FS}} = \mathbf{M_{FS}}\,\mathbf{S_i} = \frac{1}{2}\begin{bmatrix} t_{\|}^2 + t_{\perp}^2 & t_{\perp}^2 - t_{\|}^2 & 0 & 0 \\ t_{\perp}^2 - t_{\|}^2 & t_{\|}^2 + t_{\perp}^2 & 0 & 0 \\ 0 & 0 & 2t_{\|}t_{\perp} & 0 \\ 0 & 0 & 0 & 2t_{\|}t_{\perp} \end{bmatrix} \begin{bmatrix} I_i \\ Q_i \\ U_i \\ V_i \end{bmatrix} = \begin{bmatrix} I_{FS} \\ Q_{FS} \\ U_{FS} \\ V_{FS} \end{bmatrix} \tag{1}$$

where M_{FS} is the Mueller matrix for the transmission from the front surface and $t_{||}$ and $t_{\perp}$ are the Fresnel transmission coefficients corresponding to the components of linearly polarized light parallel and perpendicular to the plane of incidence. One can describe the Mueller matrix for the exit surface of the hologram in the same manner.

In order to construct the Mueller matrix for the grating itself, M_H in Figure 2, we describe the amplitude of the diffracted beam for parallel and perpendicular incidence in a manner analogous to the Fresnel reflection/transmission case. For our purposes here, we need to describe only the diffracted beam and not the transmitted component. The relevant parameters are illustrated in Figure 3. $\bar{U}_i$ is the input beam and $\bar{U}_o$ is the output beam, where $\hat{u}_i$ and $\hat{u}_o$ are the respective polarization vectors normal to the direction of propagation. $\bar{K}$ is the grating vector, which makes an angle ϕ with the z axis. We recall that the amplitude of the diffracted beam is given by[13]:

$$\frac{U_o}{U_i} = -i\alpha\,\sin\left(\sqrt{\frac{\left(\kappa\left(\hat{\mathbf{u}}_\mathbf{i}\bullet\hat{\mathbf{u}}_\mathbf{o}\right)d\right)^2}{\gamma}}\right) \tag{2}$$

$$\alpha = \sqrt{\frac{\cos\theta_i}{\cos\theta_o}} \quad \gamma = \cos\theta_i\cos\theta_o \quad \kappa = \pi n'/\lambda$$

Here, n' is the index modulation depth. For the special cases of polarizations parallel and perpendicular to the plane of incidence, the dot product in (2) can be simplified as:

$$\begin{aligned} \frac{U_o}{U_i}(d)_{\perp} &= u_{\perp} = -i\alpha\sin\left(\sqrt{\frac{\kappa^2 d^2}{\gamma}}\right) \\ \frac{U_o}{U_i}(d)_{\|} &= u_{\|} = -i\alpha\sin\left(\sqrt{\frac{\kappa^2\cos^2 2(\theta_i-\phi)d^2}{\gamma}}\right) \end{aligned} \tag{3}$$

The Mueller matrix for the hologram (M_H) and the transformation of the Stokes vector S_i are given by

$$\mathbf{S_H} = \mathbf{M_H}\,\mathbf{S_i} = \frac{1}{2}\begin{bmatrix} u_{\|}^2+u_{\perp}^2 & u_{\perp}^2-u_{\|}^2 & 0 & 0 \\ u_{\perp}^2-u_{\|}^2 & u_{\|}^2+u_{\perp}^2 & 0 & 0 \\ 0 & 0 & 2u_{\|}u_{\perp} & 0 \\ 0 & 0 & 0 & 2u_{\|}u_{\perp} \end{bmatrix}\begin{bmatrix} I_i \\ Q_i \\ U_i \\ V_i \end{bmatrix} = \begin{bmatrix} I_H \\ Q_H \\ U_H \\ V_H \end{bmatrix} \tag{4}$$

For the architecture proposed above, we must describe the diffraction amplitudes from two multiplexed gratings. These gratings must be specially designed so that they have the same Bragg angle θ_B. Following our previous analysis,[14] we can design two orthogonal gratings such that they each share the same Bragg angle. The amplitude of the diffracted beam from the j[th] grating is given as:

$$\frac{U_o}{U_i}(d)_j = -i\frac{\kappa_j(\hat{\mathbf{u}}_i \cdot \hat{\mathbf{u}}_{oj})}{\cos(\theta_{oj})\xi_0}\sin(\xi_0 d) \quad \text{for } j=1,2 \text{ where}$$

$$\xi_0 = \sqrt{\frac{1}{\cos(\theta_i)}\left[\frac{(\kappa_1(\hat{\mathbf{u}}_i \cdot \hat{\mathbf{u}}_{o1}))^2}{\cos(\theta_{o1})} + \frac{(\kappa_2(\hat{\mathbf{u}}_i \cdot \hat{\mathbf{u}}_{o2}))^2}{\cos(\theta_{o2})}\right]} \tag{5}$$

We can evaluate the parallel and perpendicular polarization cases as in (3) and obtain the proper coefficients $u_{\|}$ and $u_{\perp}$.

The proposed architecture can now be completely analyzed using the Mueller matrices found above. The Mueller matrix for one grating of the hologram is:

$$M_t = M_{ES} \cdot M_H \cdot M_{FS} \tag{6}$$

where M_{FS} is the matrix for the front surface and M_{ES} is the matrix for the exit surface. Using (1) and (4) in (6) we find that the transformation of the input Stokes vector is given by:

$$\frac{1}{2}\begin{bmatrix} A+B & A-B & 0 & 0 \\ A-B & A+B & 0 & 0 \\ 0 & 0 & 2\sqrt{AB} & 0 \\ 0 & 0 & 0 & 2\sqrt{AB} \end{bmatrix}\begin{bmatrix} I_i \\ Q_i \\ U_i \\ V_i \end{bmatrix} = \begin{bmatrix} I_t \\ Q_t \\ U_t \\ V_t \end{bmatrix} \tag{7}$$

$$A = t_{FS\perp}^2 u_{\perp}^2 t_{ES\perp}^2 \qquad B = t_{FS\|}^2 u_{\|}^2 t_{ES\|}^2$$

Equation (7) shows the Stokes vector that is diffracted from one grating. The second grating will produce an equation of the same form but with different grating coefficients *u*. Both equations have the same Stokes vector as input, but because the grating parameters *u* differ, they will produce different output. Note that using intensity detectors and given the form of the Mueller matrix in (7), we can only determine the first two Stokes parameters. In order to determine the other Stokes parameters, one must have a Mueller matrix with non-zero off-diagonal elements in the third and fourth column. This can be achieved for example by a rotation of the holographic grating about the z-

axis and by a similar rotation of the polarization axis of the incident light. This simple rotation is described by the following Mueller matrix:

$$\mathbf{M}_{RZ}(\gamma)=\begin{bmatrix}1 & 0 & 0 & 0\\ 0 & \cos 2\gamma & -\sin 2\gamma & 0\\ 0 & \sin 2\gamma & \cos 2\gamma & 0\\ 0 & 0 & 0 & 1\end{bmatrix} \tag{8}$$

This is the optimal choice because it can be realized by simply rotating the device when in use. This rotation allows us to find two equations for the two beams diffracted by the first set of multiplexed gratings:

$$\begin{aligned} I_{t1} &= I_i\left(A_1+B_1\right)+\left(Q_i\cos(2\gamma_1)-U_i\sin(2\gamma_1)\right)\left(A_1-B_1\right)\\ I_{t2} &= I_i\left(A_2+B_2\right)+\left(Q_i\cos(2\gamma_1)-U_i\sin(2\gamma_1)\right)\left(A_2-B_2\right)\end{aligned} \tag{9}$$

where the subscript 1 and 2 denote the two separate gratings. The angle γ_1 denotes the angle of rotation for gratings 1 and 2. The next set of equations comes from the beams that pass through the quarter-wave plate and diffract from the third and fourth gratings. The quarter-wave plate adds a $\pi/2$ phase shift that interchanges the U and V parameters of the Stokes vector: $\cos(\varepsilon)\rightarrow\cos(\varepsilon+\pi/2)=-\sin(\varepsilon)$ and $\sin(\varepsilon)\rightarrow\sin(\varepsilon+\pi/2)$ $=\cos(\varepsilon)$. The second set of equations is rotated an angle γ_2 and is thus:

$$\begin{aligned} I_{t3} &= I_i\left(A_3+B_3\right)+\left(Q_i\cos(2\gamma_2)+V_i\sin(2\gamma_2)\right)\left(A_3-B_3\right)\\ I_{t4} &= I_i\left(A_4+B_4\right)+\left(Q_i\cos(2\gamma_2)+V_i\sin(2\gamma_2)\right)\left(A_4-B_4\right)\end{aligned} \tag{10}$$

Because the quarter-wave plate has changed U into V, we now have four equations involving all four Stokes parameters. We are required to measure the four diffracted intensities in order to determine the Stokes parameters. The grating coefficients u and the Fresnel reflection coefficients can be measured to find the coefficient A's and B's which in turn can be used to pre-weight the detector arrays for the imaging process.

To determine the constraints on the device parameters that are required for fully determining the complete Stokes vector, we write equations (9) and (10) together in matrix form as $I_t=\mathbf{M}'S_i$. $\mathbf{M}'$ is the so-called measurement matrix, S_i is the input Stokes vector to be solved for, and I_t are the four measured intensities. For our material parameters, an example measurement matrix is given:

$$\mathbf{M}'=\begin{bmatrix}0.24320 & -0.04187 & 0.23746 & 0\\ 0.68596 & -0.03614 & 0.00637 & 0\\ 0.28996 & -0.04897 & 0 & -0.27773\\ 0.21291 & 0.11626 & 0 & 0.02050\end{bmatrix} \tag{11}$$

We have verified numerically that this matrix determines the Stokes vector robustly for a range of input values. No attempt was made to further optimize the condition[15,16] of the matrix, which requires an exhaustive search through the parameter space, and is subject to further investigation.

To summarized, we have developed a polarization imaging architecture using thick multiplexed holograms that has many advantages over current polarimetric imaging techniques. The analysis showing the principle of operation explicitly takes into account the polarization state of the incident and diffracted wave fields. Transformation of initial Stokes parameters by grating diffraction is formulated by a Mueller matrix defined in terms of diffracted amplitudes of planar and perpendicular polarization components. A procedure is outlined using two sets of rotated orthogonal gratings and a quarter-wave plate to compute all four unknown Stokes parameters required for polarimetric imaging.

References

1. J.L. Pezzaniti, and R.A. Chipman, "Mueller matrix imaging polarimetry", *Opt. Eng.* **34** 1558 (1995).
2. K.P. Bishop, H.D. McIntire, M.P. Fetrow, L. McMackin, "Multispectral polarimeter imaging in the visible to near-IR, Targets and Backgrounds: Characterization and Representation", *Proc. SPIE* **3699** 49 (1999).
3. G.P. Nordin, J.T. Meier, P.C. Deguzman, and M.W. Jones, "Micropolarizer array for infrared imaging polarimetry", *J. Opt. Soc. Am.* **A 16** 1168 (1999).
4. W.S. Bickel, W.M. Bailey, "Stokes vectors, Mueller matrices, and polarized scattered light", *Am. J. Phys.* **53** 468 (1985).
5. C. Bohren, and D.R. Huffman, "Absorption and scattering of light by small particles", *Wiley Publ.,* (1998).
6. L.J. Denes, M. Gottlieb, B. Kaminsky, and D. Huber, "Spectro-polarimetric imaging for object recognition", *Proc. SPIE*, **3240**, 8 (1998).
7. T. Nee, S.F. Nee, "Infrared polarization signatures for targets", *Proc. SPIE* **2469** 231 (1995).
8. W.G. Egan, "Polarization in remote sensing", *Proc. SPIE* **1747** 2 (1992).
9. D.W. Beekman, J.V. Anda, "Polarization sensitive QWIP thermal imager", *Infrared Physics & Tech.* **42** 323 (2001).
10. D. Kim, C. Warde, K. Vaccaro, C. Woods, "Imaging multispectral polarimetric sensor: single-pixel design, fabrication, and characterization", *Applied Optics* **42**(19) 3756-3764 (2003).
11. A. Gerrard, J.M. Burch, "Introduction to Matrix Methods for Optics", Dover Publications, NY (1974).
12. S.F.Nee, T.W. Nee, "Principal Mueller matrix of reflection and scattering measured for a one dimensional rough surface" *Opt. Eng.* **41** 994 (2002).
13. H. Kogelnik, "Coupled wave theory for thick hologram gratings", *Bell Syst. Tech. J.* **48** 2909 (1969).
14. M.S. Shahriar, J. Riccobono, M. Kleinschmit, J.T. Shen, "Coherent and incoherent beam combination using thick holographic substrates", *Optics Comm.* **220** 75-83 (2003).
15. A. Ambirajan, D.C. Look, "Optimum angles for a polarimeter", *Opt. Eng.* **34** 1651-1655 (1995).
16. D.S. Sabatke, A.M. Locke, M.R. Descour, W.C. Sweatt, J.P. Garcia, E.L. Dereniak, S.A. Kemme, G.S. Phillips, "Figures of merit for complete Stokes polarimeter optimization", *Proc. SPIE* **4133** 75-81 (2000).

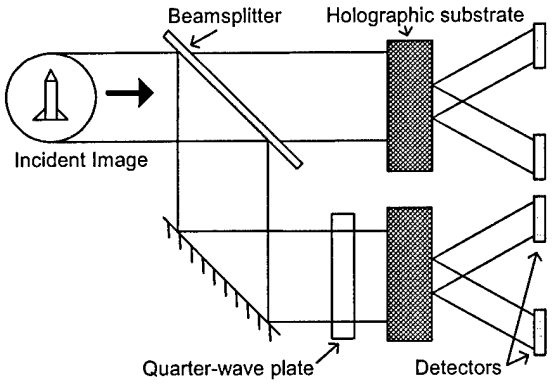

Figure 1: Schematic of the holographic Stokesmeter

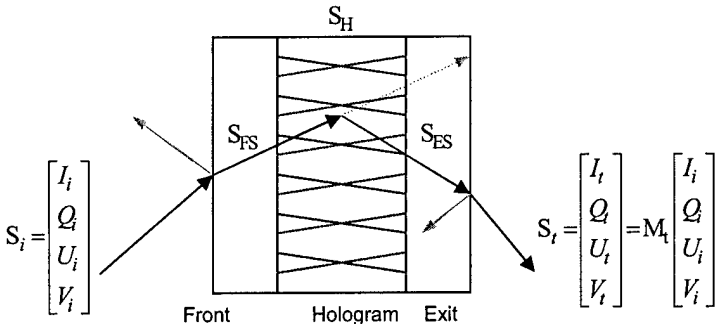

$$M_t = M_{ES} . M_H . M_{FS}$$

Figure 2: Interaction with hologram viewed in three sections

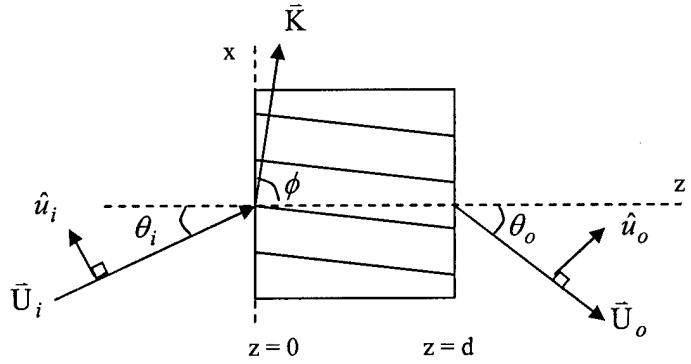

Figure 3: Diffraction from a thick, slanted grating

3.6 Publicity Articles Regarding Super-Parallel Architecture and Slow-Stopped Light.

[SEE ATTACHMENTS 5,6,7,8 FOR SAMPLES]

4. TECHNOLOGY TRANSFER:

None.